

Article

Not peer-reviewed version

# Investigating the Interactions of Peptide Nucleic Acids with Multicomponent Peptide Hydrogels for the Advancement of Healthcare Technologies

[Sabrina Giordano](#) , [Monica Terracciano](#) , [Enrico Gallo](#) , [Carlo Diaferia](#) , [Andrea P. Falanga](#) , [Antonella Accardo](#) , [Monica Franzese](#) , [Marco Salvatore](#) , [Gennaro Piccialli](#) , [Nicola Borbone](#) , [Giorgia Oliviero](#) \*

Posted Date: 2 April 2025

doi: 10.20944/preprints202504.0204.v1

Keywords: peptide nucleic acids; hydrogels; chemical functionalization; multifunctional systems; healthcare applications



Preprints.org is a free multidisciplinary platform providing preprint service that is dedicated to making early versions of research outputs permanently available and citable. Preprints posted at Preprints.org appear in Web of Science, Crossref, Google Scholar, Scilit, Europe PMC.

Copyright: This open access article is published under a Creative Commons CC BY 4.0 license, which permit the free download, distribution, and reuse, provided that the author and preprint are cited in any reuse.

## Article

# Investigating the Interactions of Peptide Nucleic Acids with Multicomponent Peptide Hydrogels for the Advancement of Healthcare Technologies

Sabrina Giordano <sup>1</sup>, Monica Terracciano <sup>2</sup>, Enrico Gallo <sup>1</sup>, Carlo Diaferia <sup>2</sup>, Andrea P. Falanga <sup>2</sup>, Antonella Accardo <sup>2</sup>, Monica Franzese <sup>1</sup>, Marco Salvatore <sup>1</sup>, Gennaro Piccialli <sup>2</sup>, Nicola Borbone <sup>2</sup> and Giorgia Oliviero <sup>3,\*</sup>

<sup>1</sup> IRCCS SYNLAB SDN, Via G. Ferraris 144, 80143, Naples, Italy

<sup>2</sup> Department of Pharmacy, University of Naples Federico II, Via D. Montesano 49, 80131, Naples, Italy

<sup>3</sup> Department of Molecular Medicine and Medical Biotechnologies, University of Naples Federico II, Via S. Pansini 5, 80131, Naples, Italy

\* Correspondence: giorgia.oliviero@unina.it

**Abstract:** This study investigates the use of peptide-based hydrogels as scaffolds for the encapsulation and delivery of Peptide Nucleic Acids (PNAs) in drug delivery applications. Ultrashort aromatic peptide-based hydrogels (HGs), such as Fmoc-FF (N $\alpha$ -fluorenyl methoxycarbonyl-diphenylalanine), provide an ideal platform for encapsulating biomolecules due to their biocompatibility, self-assembling nature, and ability to form stable, nanostructured networks. The functionalization of these hydrogels with Fmoc-FFX tripeptides—where X is cysteine (C) or lysine (K)—enhances their ability to interact with PNA sequences. Model four-bases PNA, functionalized with cysteine (C) or glutamic acid (E) residues at the C-terminus, facilitate covalent or electrostatic interactions with the hydrogel matrix, improving encapsulation efficiency and stabilizing the PNAs. We systematically optimized the composition and ratios of hydrogel components and PNAs to enhance encapsulation efficiency, structural stability, and controlled release profiles. The resulting hydrogels were thoroughly characterized using High-Performance Liquid Chromatography (HPLC), Electrospray Ionization Mass Spectrometry (ESI-MS), Circular Dichroism (CD), rheology, Fourier-Transform Infrared (FT-IR) spectroscopy, Scanning Electron Microscopy (SEM), Proton Nuclear Magnetic Resonance (<sup>1</sup>H-NMR), as well as optical and fluorescence microscopy. Our results demonstrate the potential of these hydrogels as highly effective platforms for stabilizing and delivering PNAs, offering promising prospects for the development of innovative nucleic acid-based therapies.

**Keywords:** peptide nucleic acids; hydrogels; chemical functionalization; multifunctional systems; healthcare applications

## 1. Introduction

In the rapidly evolving field of nanomedicine, the development of advanced materials capable of performing multifunctional tasks within biological systems is crucial for innovative healthcare applications. [1] Among these materials, peptide-based hydrogels have emerged as nanostructured promising candidates due to their unique combination of biocompatibility, biodegradability, and tunable physicochemical properties. [2,3] These materials mimic biological molecules, making them suitable for a wide range of applications, from tissue engineering to drug delivery, as well as biosensing applications. [4–6]

Specifically, Fmoc-FF (N $\alpha$ -fluorenyl methoxycarbonyl-diphenylalanine) is one of the most studied low molecular-weight hydrogelators, providing a foundation for the design of new peptide-based gelators with improved characteristics. [7–9]

In our previous studies, we explored the potential of the Fmoc-FF hydrogelator to form mixed hydrogels in combination with tripeptides sharing the same aromatic core and containing an additional residue of Cys, Ser, Thr, or Lys at their C-terminus. [10,11] By incorporating different quantities of the reactive functionalities, it was possible to easily obtain materials with the desired level of reactive groups on their surface, thus enhancing their interaction with bioactive molecules, such as peptide nucleic acids (PNAs), for biomedical applications.

PNAs are synthetic analogs to natural nucleic acids characterized by a backbone of *N*-(2-aminoethyl)-glycine units linked *via* amide bonds. This structure lacks the negatively charged phosphate groups, resulting in reduced electrostatic repulsion and significantly enhanced binding affinity to complementary single-stranded DNA or RNA. [12] As a result, PNAs have attracted substantial relevance in the biomedical field, acting as therapeutics exploiting the antigene, [13,14] antisense, [15–17] and anti-miRNA [18,19] approaches, as well as serving as biosensing probes in diagnostic applications. [20,21]

PNAs' enhanced binding affinity is combined with low toxicity and excellent chemical and enzymatic stability. [22] Despite these notable advantages, PNAs' limited cellular permeability and water solubility present challenges for medical applications. The development of effective delivery systems is therefore essential to address these limitations, ensuring enhanced bioavailability and therapeutic efficacy. [23,24] In this context, peptide-based hydrogels offer a compelling solution by providing a biocompatible and biodegradable scaffold that can stabilize PNA molecules and facilitate their controlled release at the target site.

In this study, we investigated peptide-based hydrogels as scaffolds for encapsulating PNAs for drug delivery applications. By directly polymerizing the hydrogels in the presence of PNAs, we systematically varied the concentrations and ratios of both the hydrogel components and PNA to optimize their properties, including encapsulation efficiency, structural stability, and controlled release profiles. This approach aims to establish hydrogels as effective and biocompatible delivery systems, highlighting their capacity to stabilize PNAs and preserve their bioactivity in complex biological environments.

We employed model PNA sequences four bases long, synthesized with and without fluorescein 5-isothiocyanate (FITC) as a fluorescent marker. Each sequence was functionalized with either a cysteine (C) or a glutamic acid (E) residue at the C-terminus, facilitating covalent or electrostatic interactions with tripeptides containing cysteine (C) or lysine (K) residues within the hydrogel matrix, respectively. This design enhanced the specificity and strength of the interactions between PNAs and the hydrogel scaffold. (Figure 1). The hydrogels were prepared using a DMSO/H<sub>2</sub>O solvent-switch approach, maintaining a 10/90 DMSO/H<sub>2</sub>O ratio. During the gelation process, the system transitioned from an opaque solution to a clear gel, as typically observed for Fmoc-FF hydrogels. This transformation highlights the ability of these systems to self-assemble into stable, nanostructured networks in aqueous environments. The resulting hydrogels were subjected to comprehensive characterization using advanced analytical techniques, including High-Performance Liquid Chromatography (HPLC), Electrospray Ionization Mass Spectrometry (ESI-MS), Circular Dichroism (CD), rheology, Fourier Transform Infrared (FT-IR) spectroscopy, Scanning Electron Microscopy (SEM), Proton Nuclear Magnetic Resonance (<sup>1</sup>H-NMR), as well as optical and fluorescence microscopies.

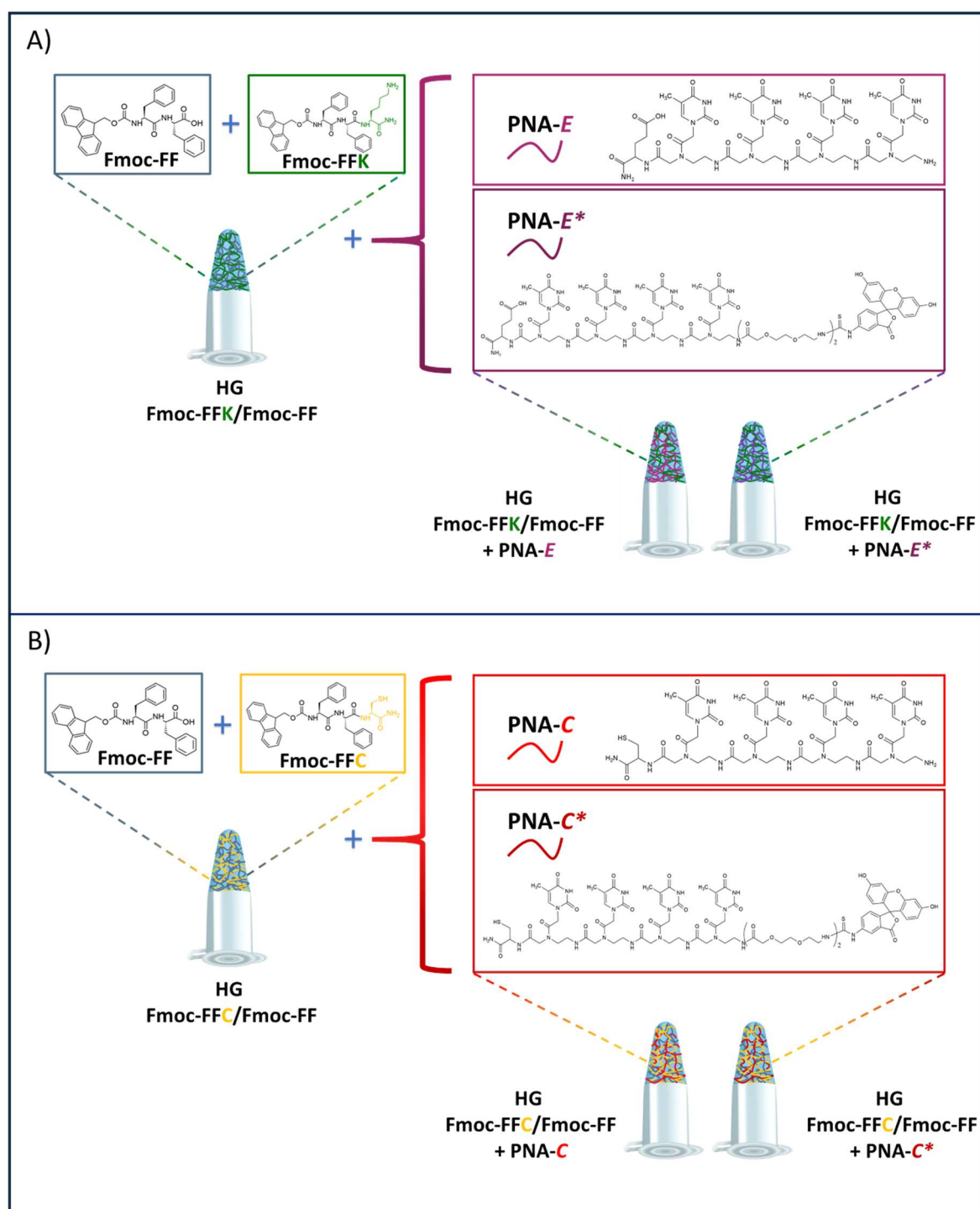


**Figure 1.** (A) Chemical structure and schematic representation of Fmoc-FF, Fmoc-FFK, and the corresponding hydrogels formed through interaction with PNA sequences containing glutamic acid (E) without or with FITC labeling, referred to as PNA-E and PNA-E\*, respectively. (B) Chemical structure and schematic representation of Fmoc-FF, Fmoc-FFC, and the corresponding hydrogels formed through interaction with PNA sequences containing Cys (C) without or with FITC labeling, referred to as PNA-C and PNA-C\*, respectively.

## 2. Results and Discussion

### 2.1. Design and Synthesis of PNA Sequences

The PNA sequences synthesized for this study (Figure 1, Table 1, Figure S1–S4) were designed to be four bases long, to facilitate a chemical investigation focused on the interactions between PNA probes and Fmoc-FF mixed hydrogels in the fabrication of tri-dimensional scaffolds with potential



biomedical applications. Fmoc-T-OH molecules were selected as monomers because pyrimidines are more suitable than purines for manual solid-phase synthesis due to their lower steric hindrance. Additionally, thymine is the only nitrogenous base that does not require protective groups, as it lacks reactive groups on its heterocyclic ring. The PNA sequences were also synthesized by incorporating a cysteine (C) or glutamic acid (E) residue as the first monomer at the C-terminus of the main chain. This design was intended to promote specific interactions between the PNA probes and the tripeptides within the hydrogels. The cysteine (C) residue was included to facilitate the formation of covalent bonds with the cysteine residue of the tripeptide, particularly through disulfide linkages. The introduction of glutamic acid (E) aimed to promote electrostatic interactions due to its negatively charged side chain, which can interact with positively charged lysine (K) residues in the tripeptides. These targeted interactions were aimed at enhancing the stability and integration of the PNA probes within the peptide-based hydrogel scaffolds. The PNA sequences were also synthesized with fluorescein 5-isothiocyanate (FITC) labeling at the N-terminus to facilitate a better understanding of hydrogel formation. This labeling is instrumental for observing the interactions between the PNA probes and the peptide hydrogels, offering valuable insights into the dynamics of hydrogel assembly. The high absorptivity and fluorescence quantum yield of FITC enable sensitive detection of the PNA sequences during optical measurements. To improve water solubility, two units of the PEG<sub>2</sub> spacer were also inserted between the FITC and the tetra-thymine framework.

**Table 1.** Sequences of PNAs used in this study.

Sample	Sequence (C→N)	Chemical formula	M.W. calc. (a.m.u.)	M.W. det. (a.m.u.)	Rt (min)
PNA-E	E – t <sub>4</sub> – NH <sub>2</sub>	C <sub>49</sub> H <sub>65</sub> N <sub>17</sub> O <sub>20</sub>	1211.46	1211.6	11.2
PNA-E*	E – t <sub>4</sub> – (PEG2) <sub>2</sub> – FITC	C <sub>82</sub> H <sub>98</sub> N <sub>20</sub> O <sub>31</sub> S	1891.64	1891.7	16.4
PNA-C	C – t <sub>4</sub> – NH <sub>2</sub>	C <sub>47</sub> H <sub>64</sub> N <sub>18</sub> O <sub>17</sub> S	1185.44	1185.5	11.6
PNA-C*	C – t <sub>4</sub> – (PEG2) <sub>2</sub> – FITC	C <sub>80</sub> H <sub>97</sub> N <sub>21</sub> O <sub>28</sub> S <sub>2</sub>	1865.63	1865.7	16.2

PNA bases are in lowercase letters.

2.2. Design and Synthesis of Peptide Building Blocks

To ensure high chemical homology, the tripeptide design should be ensured by a minor disruption of the previously identified non-covalent contact pathways responsible for both aggregation and gelation, as demonstrated in our previous studies. [10,11] Among the twenty natural amino acids, cysteine (C) and lysine (K) were selected to promote interactions with the synthesized PNAs. These functional entities can be efficiently employed for post-aggregation functionalization, facilitating the creation of responsive systems tailored for biomedical applications, including biosensing and drug delivery. [25] The two tripeptides (Fmoc-FFC and Fmoc-FFK) were synthesized and purified using conventional solid-phase peptide synthesis (SPPS) standard protocols and RP-HPLC chromatography. ESI mass spectrometry, <sup>1</sup>H-NMR spectroscopy, and analytical HPLC characterization were then used to confirm their identity. [10,11] These tripeptides retain the Fmoc-FF motif but additionally have a residue at the C-terminal end that gives the resulting hydrogel additional properties that allow it to be functionalized with biologically active compounds.

2.3. Hydrogels Formulation

To generate hydrogels, the synthesized tripeptides were combined with the Fmoc-FF and PNA molecules. The Fmoc-FFX sequences were mixed with Fmoc-FF at different ratios (1/1, 1/5, 1/10, and 1/20 w/w for Fmoc-FFX/Fmoc-FF, where X = C or K), as previously evaluated for mixed matrices. [10,11] To achieve hydrogels with varying degrees of functionalization, the tripeptide content within the mixed matrices was intentionally reduced in a stepwise manner. Subsequently, hybrid hydrogels were produced by using the solvent-switch approach while maintaining a constant DMSO/H<sub>2</sub>O ratio

(10/90,  $\phi_{\text{solvent}} = 0.10\%$ ). [26] The addition of water caused the metastable solution to switch from opaque to clear, in agreement with the expected behavior of Fmoc-FF-based hydrogels. [27] To promote the incorporation of the PNA molecules into the mixed hydrogels, the solvent-switch method was slightly modified. The PNA molecules were dissolved in doubly filtered MilliQ water, and these solutions of known concentration were then used to formulate the mixed hydrogels by the solvent-switch method (Figure 2). Due to the increase of opacity associated with the gel formation process, the absorbance spectra of the samples at 600 nm (long-range) were measured over time at set intervals to quantitatively determine the kinetics of gels' formation. In this way, it was possible to identify the gelation times ( $G_t$ ) corresponding to the inflection point of the curves (Figure S5), as all samples show a decrease in optical density (OD) during the transition from opaque to clear. The amount of tripeptide relative to Fmoc-FF does not appear to be the sole factor influencing the gelling kinetics, as shown by the gelation times listed in Table 2. The incorporation of PNA molecules generally leads to extended formation times for all samples, with the notable exception of the Fmoc-FFK/Fmoc-FF 1/20 + PNA-E system, where the gelation time is markedly reduced. This observation suggests that factors such as heteroatoms, steric hindrance, and the presence of PNA may play a significant role in influencing gel formation. Specifically, steric hindrance is particularly pronounced in the Fmoc-FFK/Fmoc-FF 1/20 + PNA-E\* sample, which exhibits no gelation (Figure 2A), emphasizing how this factor can substantially hinder the gelating process.

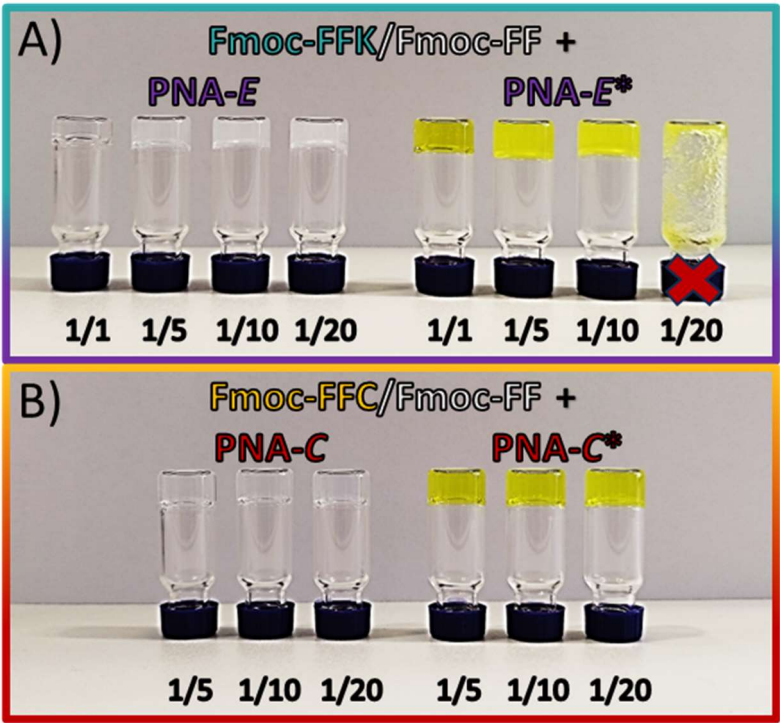


**Figure 2.** Inverted test tube for 400  $\mu\text{L}$  of mixed hydrogel formulations (1.0 wt%) of (A) Fmoc-FFK/Fmoc-FF HGs, at different ratios (1/1, 1/5, 1/10, 1/20,  $w/w$ ) with 0.15 mM PNA-E (left) and 0.15 mM PNA-E\* (right) solutions and (B) Fmoc-FFC/Fmoc-FF HGs, at different ratios (1/5, 1/10, 1/20,  $w/w$ ) with 0.15 mM PNA-C (left) and 0.15 mM PNA-C\* (right) solutions.

**Table 2.** Characterization of mixed hydrogels at different  $w/w$  ratios. Gelation times ( $G_t$ ) of mixed hydrogels with and without PNAs addition.

System (HG)	Ratio with Fmoc-FF ( $w/w$ )	Gelation Time (min)	Gelation Time of solely HGs (min)
Fmoc-FFK/Fmoc-FF + PNA-E [50 $\mu\text{M}$ ]	1/1	26	10
	1/5	112	78
	1/10	164	138

	1/20	34	216
	1/5	80	75
Fmoc-FFC/Fmoc-FF + PNA-C	1/10	25	4
[50μM]	1/20	10	2

#### 2.4. Rheology

The obtained systems showed self-supporting properties suggesting the formation of non-Newtonian behavior. [28] The resulting materials were evaluated in their mechanical response *via* rotational rheological analysis, reporting the viscoelastic profile (Figure S6) for each Fmoc-FFX-containing PNA [50 μM] in terms of  $G'$  (storage modulus) and  $G''$  (loss modulus). The analysis was conducted by performing a dynamic oscillation strain sweep (at a frequency of 1.0 Hz), extrapolating moduli values at  $\omega = 0.1\%$  (Table 3).

**Table 3.** Rheological analysis of hydrogels loaded with PNAs. Reported data are storage modulus ( $G'$ ), loss modulus ( $G''$ ), and  $\tan \delta$  ( $G'/G''$ ).

Fmoc-FFK/Fmoc-FF + PNA-E				Fmoc-FFC/Fmoc-FF + PNA-C			
Ratio with Fmoc-FF	$G'$ (Pa)	$G''$ (Pa)	$\tan \delta$	Ratio with Fmoc-FF	$G'$ (Pa)	$G''$ (Pa)	$\tan \delta$
1/1	140	20	0.143				
1/5	19320	1770	0.0920	1/5	648	112	0.173
1/10	6243	444	0.0710	1/10	6941	1019	0.147
1/20	8711	486	0.0557	1/20	22471	2371	0.105

The  $G' > G''$  relationship, as the consequent  $\tan \delta$  ( $G''/G'$ )  $< 1$ , analytically demonstrates the gel state of all the tested matrices, with a preference for elastic dissipation of the applied torque force. The linear viscoelastic region (LVE region) for both Fmoc-FFK- and Fmoc-FFC-containing matrices was found in the 0.01–8.0% strain range, in line with empty peptide-based hydrogels. [10,11] An increase of  $G'$  with the amount of Fmoc-FF component was observed only for Fmoc-FFC-containing matrices. Fmoc-FFC-based HGs are more rigid at higher percentages of Fmoc-FF and less rigid at lower percentages of Fmoc-FF, suggesting that the amount of Fmoc-FF deeply affects the rigidity. Otherwise, a progressive decrease of  $\tan \delta$  with the increase of the Fmoc-FF component was detected. This suggests possible cooperative interaction between the Fmoc-FF component and PNA. This interaction may affect the mesh size, with a progressive increase in the elastic's component rheological response. [29] Indeed,  $G'$  values rise as the tripeptide/Fmoc-FF ratio increases and with the addition of PNA molecules, indicating a corresponding increase in the stiffness of the filled hydrogels. This effect is likely due to the gelation properties of Fmoc-FF, which reassembles into denser networks within the matrices, resulting in the formation of more rigid structures. [30,31]

#### 2.5. Hydrogel Stability Studies

The stability of empty and filled HGs was evaluated over time (up to 7 days) by incubating them in the Ringer's solution at 40 °C and by further evaluating their weight loss. [32] The obtained results are reported in Table 4 for empty HGs and Table 5 for PNA-filled HGs. The values expressed by  $\Delta W(\%)$ , indicate a low weight loss for all the hydrogels ( $< 4.0\%$ ), indicating a high level of stability.

**Table 4.** Stability Test of empty hydrogels.

Fmoc-FFK/Fmoc-FF				Fmoc-FFC/Fmoc-FF			
Ratio with Fmoc-FF	$W_0$ (g)	$W_t$ (g)	$\Delta W (\%)$	Ratio with Fmoc-FF	$W_0$ (g)	$W_t$ (g)	$\Delta W (\%)$

1/1	1.3438	1.3263	1				
1/5	1.3411	1.3200	2	1/5	1.3362	1.3229	1
1/10	1.3320	1.3290	0	1/10	1.3429	1.3298	1
1/20	1.3363	1.2979	3	1/20	1.3417	1.3393	0

**Table 5.** Stability Test of hydrogels loaded with PNAs.

<i>Fmoc-FFK/Fmoc-FF + PNA-E</i>				<i>Fmoc-FFC/Fmoc-FF + PNA-C</i>			
Ratio with Fmoc-FF	$W_0$ (g)	$W_t$ (g)	$\Delta W$ (%)	Ratio with Fmoc-FF	$W_0$ (g)	$W_t$ (g)	$\Delta W$ (%)
1/1	1.3023	1.2849	1				
1/5	1.3280	1.3089	1	1/5	1.2802	1.2244	4
1/10	1.3266	1.3034	2	1/10	1.2927	1.2401	4
1/20	1.3306	1.2869	3	1/20	1.3015	1.2519	4

## 2.6. Swelling Kinetics

Swelling is a specific characteristic of gelated matter. Macroscopically, swelling represents the volumetric growth of a porous network with the resulting increase in weight due to water entrapment. For all matrices tested, the swelling kinetics were studied for 24 hours by evaluating the swelling ratios ( $q$ ), reported as a percentage and correlated with weight gain (see Figure S7 and S8). All samples reached a plateau around 4 hours and after 24 hours the swelling ranged between 34.8% and 38.7% (Tables 6 and 7). As expected for multi-component matrices, the  $q$ -values are higher than those of the pure Fmoc-FF hydrogel (29%). No substantial differences are visible between the samples. Only a slight increase in swelling properties can be revealed for the PNA-loaded samples, suggesting a role of this component in water retention.

**Table 6.**  $q$  values (%) at 24 h for empty matrices.

Sample (Empty HGs)	Ratio with Fmoc-FF	$q$ (%)
Fmoc-FFK/Fmoc-FF	1/1	36.1
	1/5	36.8
	1/10	35.0
	1/20	34.8
Fmoc-FFC/Fmoc-FF	1/5	38.7
	1/10	37.2
	1/20	36.2

**Table 7.**  $q$  values (%) at 24 h for PNA loaded matrices.

Sample (Loaded HGs)	Ratio with Fmoc-FF	$q$ (%)
Fmoc-FFK/Fmoc-FF + PNA-E	1/1	37.7
	1/5	37.7
	1/10	37.3
	1/20	37.9
Fmoc-FFC/Fmoc-FF + PNA-C	1/5	36.7
	1/10	36.9
	1/20	37.9



## 2.7. Multicomponent PNA-Hydrogels' Secondary Structure Characterization

To identify and eventually compare the occurrence of possible changes in the architecture of multicomponent hydrogels combined with PNA molecules, structural assessments were performed *via* CD, FT-IR, <sup>1</sup>H-NMR, and SEM.

### 2.7.1. Circular Dichroism Spectroscopy (CD)

The secondary structure adopted by peptides within the hydrogel matrices was examined using CD measurements and compared with previously reported structures for standalone mixed multicomponent hydrogels. [10,11] Upon evaluating Figure 3A, it is possible to assess that there are no noteworthy distinctions between the tested samples and the CD profiles of the hydrogels without PNA. For each of them,  $\pi \rightarrow \pi^*$  transitions are responsible for the detection of a positive band detectable around 195 nm and a negative band centered between 205 and 210 nm. [33,34] Additionally, a signal around 230 nm is indicative of a super-helical organization of the phenylalanine residues, as previously evidenced for pristine Fmoc-FF hydrogels. [35] The broad band at 270–280 nm indicates that this arrangement causes the fluorenyl moieties in the hydrogels to have a helical-like orientation. [36] Comparing the CD spectra, the signal of the hydrogels with PNAs trapped inside is reduced. This is supported by evidence showing that the PNA component displays little to no dichroic signal (Figure S9).

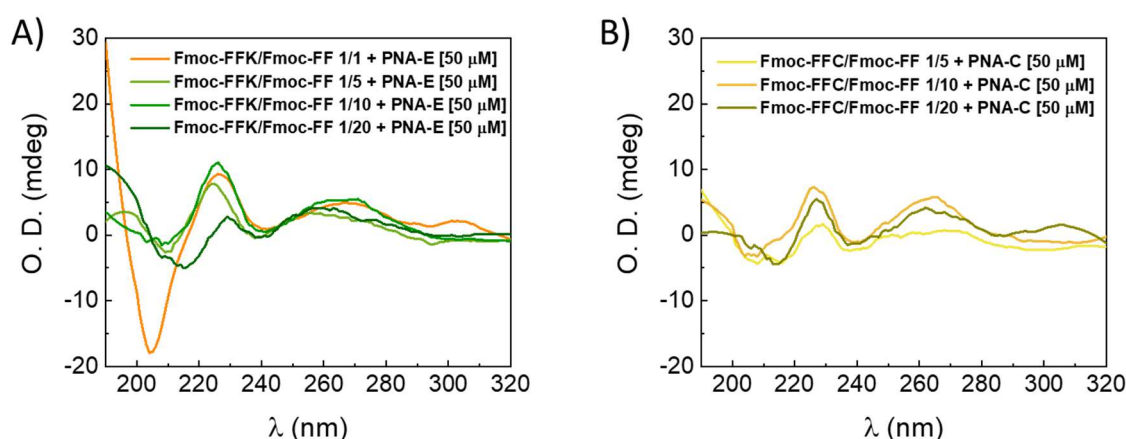


**Figure 3.** CD spectra (range 190–320 nm) of (A) Fmoc-FFK/Fmoc-FF (1.0 wt%) at different *w/w* ratios (1/1, 1/5, 1/10, 1/20) with PNA-E [50 μM] and (B) Fmoc-FFC/Fmoc-FF (1.0 wt%) at different *w/w* ratios (1/5, 1/10, 1/20) together with PNA-C [50 μM].

### 2.7.2. Fourier Transform Infrared Spectroscopy (FT-IR)

FT-IR spectroscopy analysis was also used to further characterize the structural organization of peptides inside the mixed hydrogels filled with PNA molecules. Figure 4 collects the amide I region (range 1700–1600  $\text{cm}^{-1}$ ) of mixed HGs combined with PNA molecules dissolved in water, presented as an absorbance spectrum. Examining the FT-IR spectra reported, three main peaks can be distinguished at ~1690, 1642, and 1630  $\text{cm}^{-1}$ , attributable to  $\beta$ -sheet conformations. [37,38] The presence of a peak at 1660  $\text{cm}^{-1}$  refers to minor  $\alpha$ -helical-like structuring, which is less intense as the Fmoc-FFK component within the hydrogels increases. [39] The formulations under study represent the two extremes in terms of Fmoc-FFK concentration. No noteworthy changes involving the secondary structure were found, thus suggesting that the arrangement is the same for 1/5 and 1/10 *w/w* ratios as well. The FT-IR spectrum obtained for the system containing cysteine shows the same behavior as the system shown below, thus confirming the same structuring of the PNA-filled hydrogel. The control spectra of PNA-E and PNA-C alone at a concentration of 50 μM are shown in the Supplementary Information as Figure S10 (A,B).

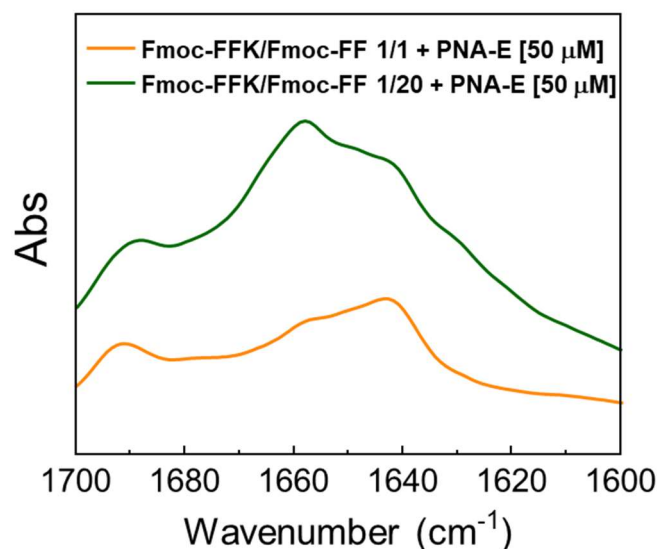


**Figure 4.** FT-IR absorbance spectra in the Amide I region (range 1700–1600  $\text{cm}^{-1}$ ) of Fmoc-FFK/Fmoc-FF (1.0 wt%) at the two most extreme  $w/w$  ratios (1/1, 1/20) with PNA-E [50  $\mu\text{M}$ ].

### 2.7.3. Peptides and PNAs $^1\text{H}$ -NMR Spectroscopy

We recorded the proton NMR spectra at 298 K for the pure peptides (Figure S11 and Figure S12) and PNAs (Figure S13 and Table S1), as well as for the hydrogels resulting from their combination (Figure 5 and Figure 6). While the pure products were thoroughly characterized, the same level of characterization could not be achieved for the hydrogels using this technique. Liquid NMR proved unsuitable for characterizing hydrogels due to their high viscosity and semi-solid nature. The restricted molecular motion in gels leads to broad, poorly resolved signals, and their longer relaxation times result in low signal-to-noise ratios. However, one key observation that confirmed the encapsulation of PNA in the hydrogel for both samples was the appearance of new signals that were not present in the hydrogel alone (Fmoc-FFK/Fmoc-FF and Fmoc-FFC/Fmoc-FFC). These signals, located in the regions between 7.5 and 7 ppm and from 5 to 1.5 ppm, are indicative of the successful encapsulation of the PNA, providing clear evidence of its incorporation into the hydrogel matrix (Figures 5 and 6). Unfortunately, the assignment of the signals was not possible due to the reasons explained above.

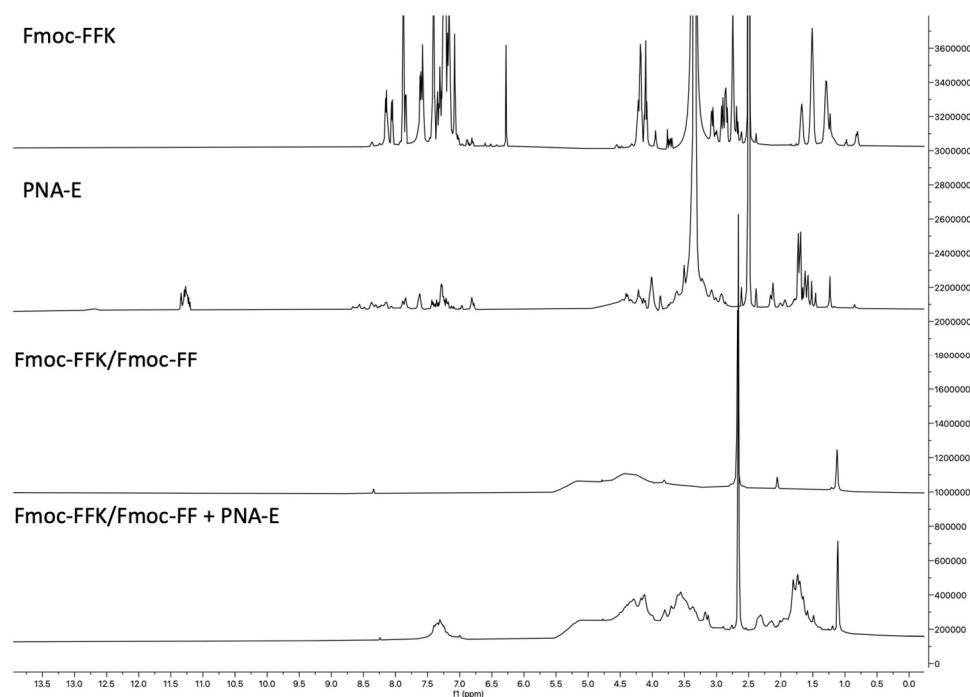


**Figure 5.** <sup>1</sup>H-NMR spectra of Fmoc-FFK, PNA-E, Fmoc-FFK/Fmoc-FF and Fmoc-FFK/Fmoc-FF+PNA-E hydrogel in DMSO-d<sub>6</sub>.

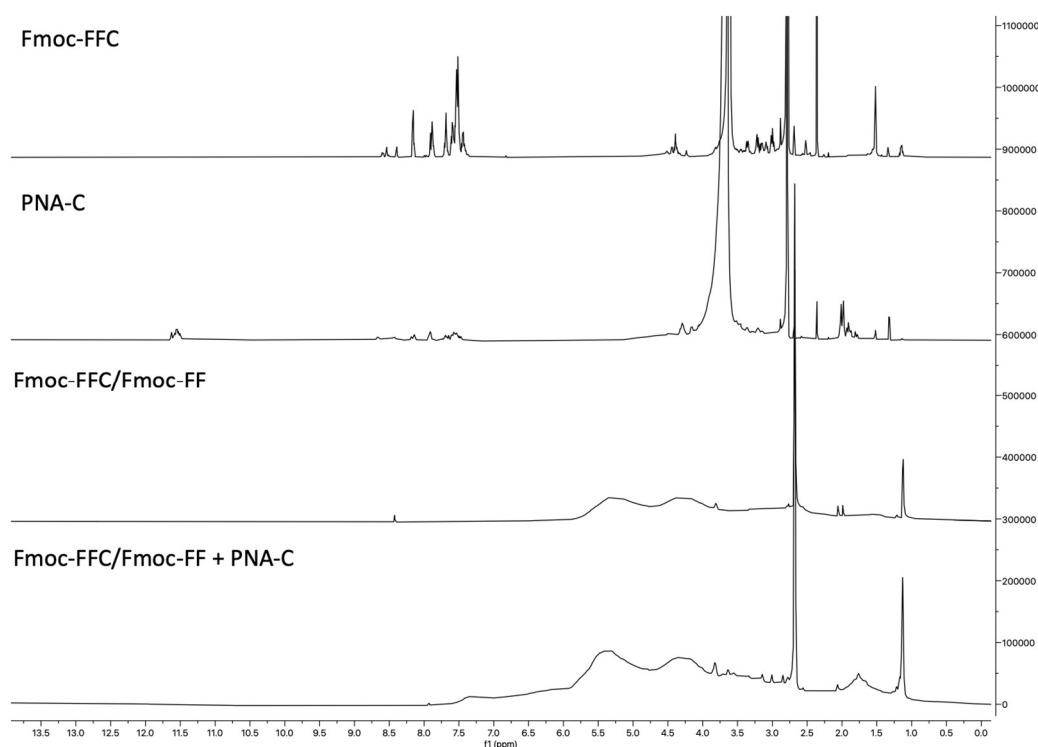


**Figure 6.** <sup>1</sup>H-NMR spectra of Fmoc-FFC, PNA-C, Fmoc-FFC/Fmoc-FF and Fmoc-FFC/Fmoc-FF+PNA-C hydrogel in DMSO-d<sub>6</sub>.

#### 2.7.4. Fluorescence Spectroscopic Assay

This assay sheds light on the localization of labeled probes trapped in hydrogels, such as the PNA molecules. [40] The spectroscopic assay was performed on xerogels, prepared by drying preformed gels combined with PNAs [25 μM] on a clean slide glass. This PNA concentration was selected as the previously tested concentration [50 μM] exhibited a high background signal, hindering accurate visualization of the samples in fluorescence imaging. As can be seen from the

images, the fluorescence is due to the FITC fluorophore covalently bound to the PNA main chain, which reduces the steric hindrance on the molecule. It is noticeable that the PNA molecules are homogeneously distributed within the three-dimensional matrix of the hydrogels (Figure 7). Moreover, the pores observed in the gels form during the drying process, a common phenomenon when preparing hydrogels for microscopy, due to the dehydration caused by drying.

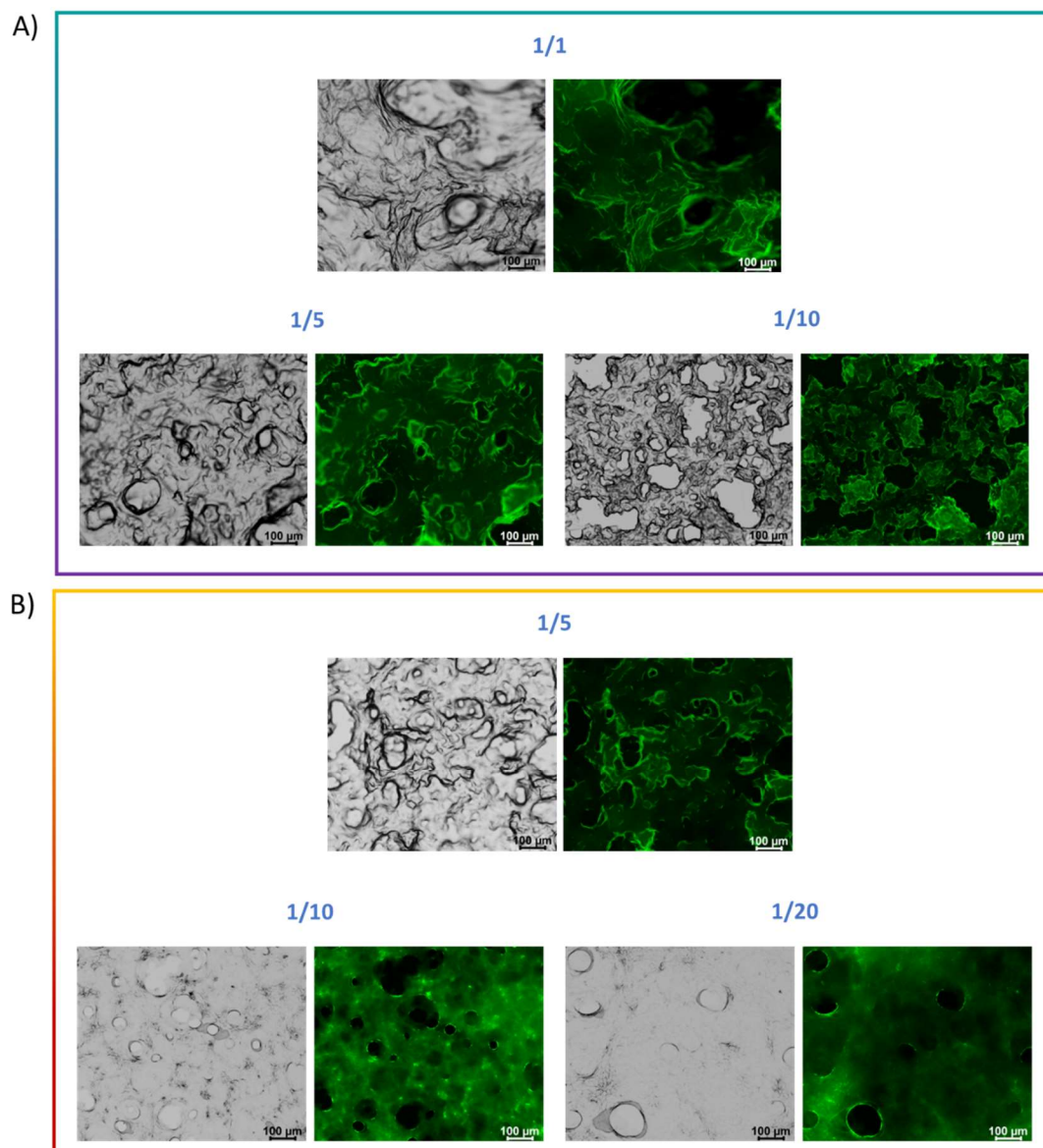


**Figure 7.** Fluorescence images of multicomponent xerogels mixed with PNA-FITC solution [25  $\mu$ M] under bright field and in the green fluorescent protein spectral region ( $\lambda_{exc} = 488$  nm). (A) Fmoc-FFK/Fmoc-FF (1.0 wt%) at different  $w/w$  ratios (1/1, 1/5, 1/10) with PNA-E\* [25  $\mu$ M]; (B) Fmoc-FFC/Fmoc-FF (1.0 wt%) at different  $w/w$  ratios (1/5, 1/10, 1/20) together with PNA-C\* [25  $\mu$ M]. Scale bars are 100  $\mu$ m for all the pictures.

#### 2.7.5. Scanning Electron Microscopy (SEM)

SEM was employed to assess the topography and morphology of the supramolecular components constituting the hydrogel matrices, along with the PNAs encapsulated within them. Figure 6 displays representative SEM photomicrographs, demonstrating that each sample is free of long, unbranched fibers, a type of entanglement frequently seen in peptide hydrogels. [41] Indeed, earlier characterizations performed solely on peptide hydrogels verified this underlying structure. [10,11] On the other hand, by adding PNAs into the hydrogels' matrix, a more rounded shape is noticeable, possibly due to the presence of trapped PNA molecules within the peptides' network.[42]

The two sequences of PNA used in this study were investigated without the hydrogels under the scanning electron microscope as well. From the SEM micro photos in Figure 6 H,I, it can be observed that even the PNA alone has a propensity to self-assemble into large amorphous aggregates.

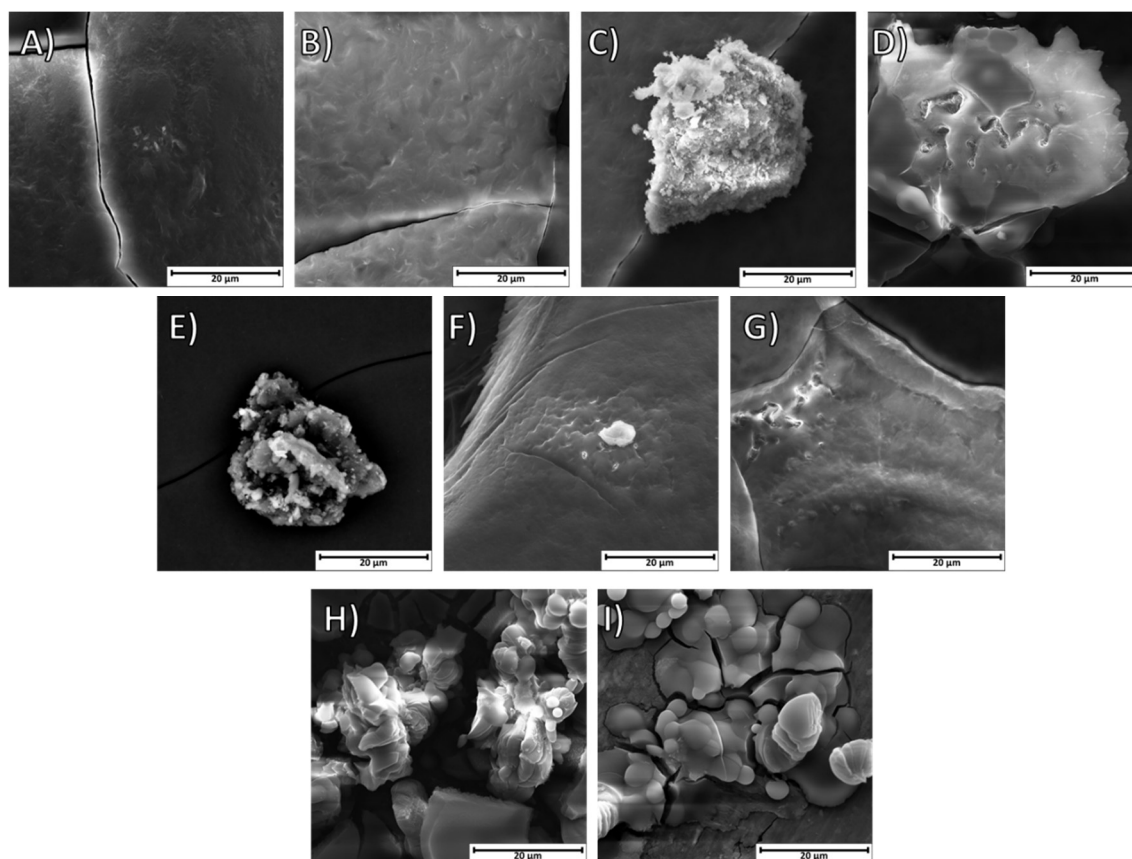


**Figure 6.** Selected micro photos of multicomponent xerogels mixed with [50µM] PNA: Fmoc-FFK/Fmoc-FF at (A) 1/1, (B) 1/5, (C) 1/10, and (D) 1/20 *w/w* ratios; Fmoc-FFC/Fmoc-FF at (E) 1/5, (F) 1/10, and (G) 1/20 *w/w* ratios; PNA-E alone (H) and PNA-C alone (I). Scale bars: 20 µm for all the pictures.

### 2.8. Release and Permeation Studies of PNAs

The capability of multicomponent hydrogels to retain drug molecules and thus serve as reservoirs for controlled drug release was tested by encapsulating PNA molecules within the matrices and evaluating the release over time. Two systems were taken under consideration for these studies: Fmoc-FFC HGs coupled with PNA-C\* and Fmoc-FFK HGs interacting with PNA-E\*. The release profile of PNA-FITC molecules from the hydrogels was efficiently monitored using UV-vis spectroscopy. During the rehydration phase of the solvent switch formulation procedure, a total of [0.15 mM] PNA-FITC was retained within the hydrogel networks. Following quantitative PNA-FITC loading, no syneresis was seen. Figure 7A, C reports PNA release kinetics over a period of 10 days. Fmoc-FFK/Fmoc-FF 1/20 was not included in the current investigation as the hydrogel precipitated at the abovementioned PNA-E\* concentration, thus preventing the appropriate gel formation. For PNA-E\* loaded hydrogels prepared by mixing Fmoc-FFK and Fmoc-FF at 1/1 and 1/5 *w/w* ratios, it can be observed similar release behaviors, which are 53% and 45%, respectively. On the contrary, the release significantly increases (up to 90%) in the Fmoc-FFK/Fmoc-FF 1/10 HG.



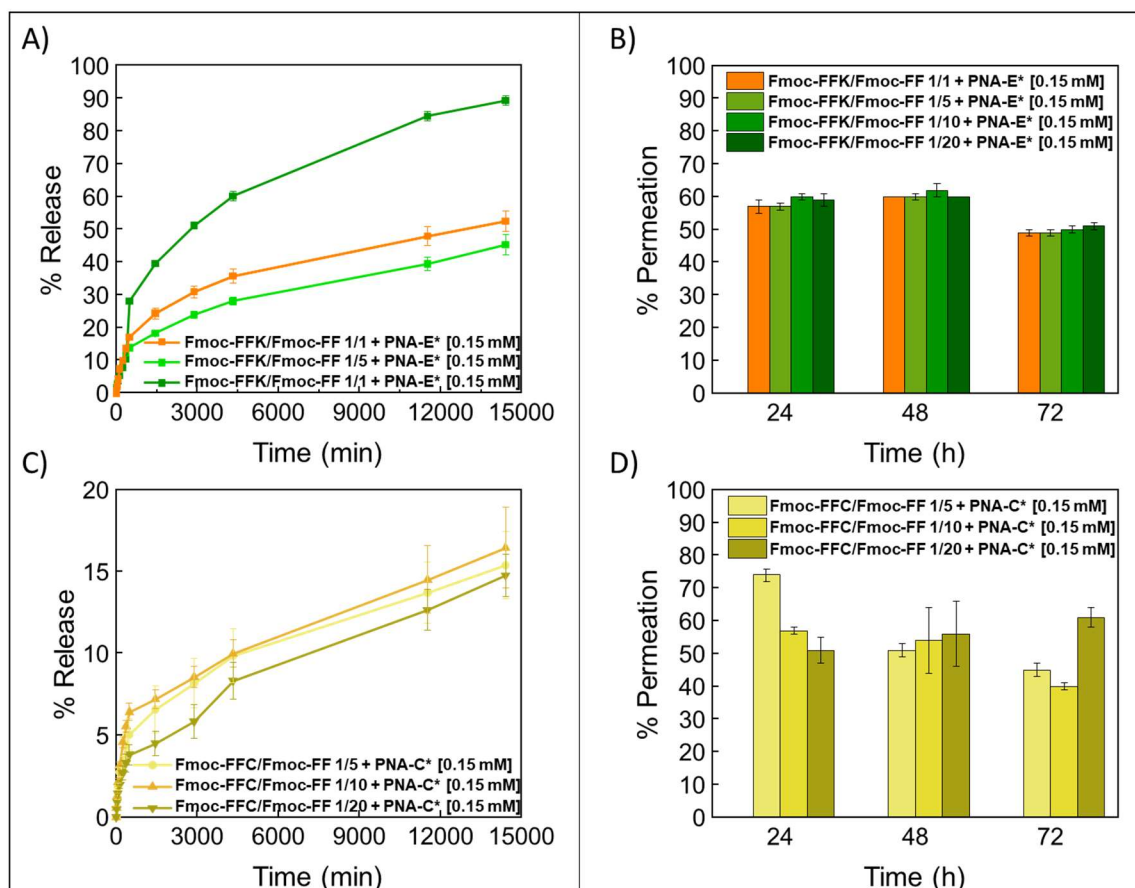


**Figure 7.** The release kinetics of PNA-E\* and PNA-C\* solutions [0.15 mM] over 10 days are reported (A,C). This solution was used to formulate 400  $\mu$ L of the Fmoc-FFK and Fmoc-FFC hydrogels at different  $w/w$  ratios together with Fmoc-FF. Permeation assays were carried out by incubating Fmoc-FFK and Fmoc-FFC hydrogels (400  $\mu$ L) at different weight ratios with Fmoc-FF (1/1, 1/5, 1/10, and 1/20) with 800  $\mu$ L PNA-E\* and PNA-C\* solutions [0.15 mM] over 72 hours (B,D).

Regarding the system involving Fmoc-FFC and PNA-C\* hydrogels, the three gels at different weight ratios (1/5, 1/10, and 1/20) displayed a lower release rate compared to PNA-E\*+Fmoc-FFK/Fmoc-FF (~15%), over the same period. This may be due to limited diffusion of the reducing agent within the hydrogel matrix, which could have hindered complete disulfide bond cleavage.

On the other hand, permeation studies with PNA-FITC derivatives were also carried out on the empty HGs using the same concentrations of PNA-FITC solutions. Permeation was monitored at three time points (24, 48, and 72 hours), and the results are shown in Figure 7B, D. Despite the different weight ratios between the lysine-containing hydrogels, the former system showed a similar permeation rate (~50% after 72 h) for all samples. From the comparison of the permeation rate over time, it seems that there is a slight, not significant, decrease in the permeation over time. Instead, Fmoc-FFC mixed HGs showed a permeation rate of 45%, 40%, and 60% for the 1/5, 1/10, and 1/20  $w/w$  ratios, respectively. In this case, it can be observed a variation of the PNA-C\* molecule as a function of both the time and the HG composition. The overall findings highlight the possibility that stiffness and electrostatic interactions are not the only variables that affect drug retention.

One reasonable explanation is that the fluorophore's propensity to escape or to be retained from HG may be influenced by the matrix's varying hydrophilic and hydrophobic properties, which result in varying degrees of water accessibility.

### 3. Conclusions

In conclusion, the innovative system we developed, based on the combination of PNA sequences and peptide hydrogels, represents a promising strategy for drug delivery applications. By leveraging the sequence-specific recognition of PNA and the biocompatible, tunable properties of hydrogels, this platform offers a controlled and selective approach to therapeutic molecule delivery. We optimized the formulation of hydrogels in the presence of PNAs for more controlled and efficient release profile. Among all the formulations tested, the 1/10 ratio proved to be the most effective for both the HG systems because this specific ratio ensures an optimal balance between structural stability and release properties, thus resulting in a more efficient release than the other compared ratios. On the other hand, regarding permeation conditions, the 1/20 ratio formulations proved to be the most effective for both systems tested. Indeed, this specific ratio ensured an easier permeation of the model PNAs. The results indicate that the 1/20 ratio offers ideal conditions for improved permeation performance, making it the best choice among the formulations tested. Moreover, the results from stability and swelling tests indicate that the multi-component matrices behave efficiently in terms of water retention and stability in harsh solvents. These results imply that the incorporation of various components into the matrices can greatly enhance the filled properties of hydrogels, with potentially advantageous implications for biomedical applications, as controlled release systems, even though the differences between the samples are negligible.

These findings highlight the potential of this system for drug delivery applications, especially in contexts where controlled release and targeted delivery are essential. Thanks to the modularity and distinctive physicochemical properties, the current system stands out from existing solutions by combining the advanced functionality of PNA with the high biocompatibility of hydrogels.

While these preliminary results have established a solid foundation for efficient hydrogel formation and PNA encapsulation, further optimization is necessary, particularly regarding tumor treatment applications. Future studies will focus on *in vitro* and *in vivo* evaluations to assess the hydrogel's performance under biologically relevant conditions, paving the way for its future use in targeted drug delivery.

### 4. Materials and Methods

#### 4.1. Chemicals and Reagents

Protected  $N^{\alpha}$ -Fmoc-amino acids, coupling reagents and Rink amide MBHA (4-methylbenzhydrylamine) resin were purchased from Calbiochem-Novabiochem (Läufelfingen, Switzerland). Fmoc-FF peptide was bought from Bachem (Bubendorf, Switzerland).  $N$ -(2-(((9H-fluoren-9-yl)methoxy)-carbonyl)amino)ethyl)- $N$ -(2-(5-methyl-2,4-dioxo-3,4-dihydropyrimidin-1(2H)-yl)acetyl)glycine (Fmoc-PNA-T-OH) as well as the spacer [2-(2-(Fmoc-amino)ethoxy)ethoxy]acetic acid (Fmoc-PEG<sub>2</sub>-OH) were purchased from LGC Biosearch Technologies™ (Scotland). Dithiothreitol (DTT) from Merck (Milan, Italy). All other chemical products are commercially available from Merck (Milan, Italy), Fluka (Bucks, Switzerland), or LabScan (Stillorgan, Dublin, Ireland) and, unless stated otherwise, were used as delivered by the companies.

#### 4.2. PNA and Peptides Synthesis, Purification, and Analysis

PNA sequences (Table 1) were synthesized using the 9-fluorenylmethoxycarbonyl (Fmoc) solid-phase strategy, following the protocol reported elsewhere. [13] The last two coupling processes were carried out for two hours each prior to the detachment from the resin to covalently bind two spacer molecules (Fmoc-PEG<sub>2</sub>-OH) at the  $N$ -terminus on the PNA-C\* and PNA-E\* main chains. At the end of the synthesis, PNA sequences were left under stirring for 3 h into a solution of Trifluoroacetic acid (TFA)/triisopropylsilane (TIS)/1,2-ethanedithiol/H<sub>2</sub>O (92.5/2.5/2.5/2.5 *v/v/v/v*), to promote the detachment from the resin. Then, the PNAs underwent a precipitation step, performed in cold diethyl

ether and after this, three cycles of lyophilization. The raw product was purified by semipreparative HPLC analyses by Jasco (Easton, MD, USA) Plus pump equipped with a Jasco UV-2075 Plus UV detector using a 10 × 250 mm C-18 reverse-phase column (particle size 5 µm) (Merck Millipore Billerica, MA, USA) eluted with a linear gradient of CH<sub>3</sub>CN containing 0.1% (*v/v*) TFA in H<sub>2</sub>O containing 0.1% (*v/v*) TFA (from 0 to 100% in 45 min, flow 1.2 mL min<sup>-1</sup>). The purified PNA was lyophilized using a SCANVAC Cool Safe 55 freeze-dryer (ScanLaf A/S, Lyngby, Denmark) by setting the freezing-temperature at -65 °C, vacuum pressure at 0.01 mbar, and heating temperature at +100 °C. After the lyophilization process, the samples were dissolved in pure water estimating the concentration by UV analyses by the Jasco V-530 spectrophotometer ( $\lambda$  = 220–310 nm, 400 nm min<sup>-1</sup> scanning speed, 2.0 nm bandwidth;  $\epsilon_{(260)}$  = 35200 cm<sup>-1</sup>M<sup>-1</sup> for PNA-C and PNA-E;  $\epsilon_{(260)}$  = 48900 cm<sup>-1</sup>M<sup>-1</sup> for PNA-C\* and PNA-E\*. The products were characterized by ESI-MS Applied Biosystems 4000 QTRAP mass spectrometer. Fmoc-FFK and Fmoc-FFC tripeptides were synthesized according to standard solid-phase peptide synthesis (SPPS) procedures using the Fmoc/*t*Bu strategy [43] as previously described. [10,11]

#### 4.3. Hydrogels Formulation

Samples and peptide-based hydrogels were prepared by weight using dimethyl sulfoxide (DMSO) and double-distilled water. All mixed hydrogels were formulated at a concentration of 1.0 wt% (10 mg·mL<sup>-1</sup>) *via* DMSO/H<sub>2</sub>O solvent-switch method by using different *w/w* ratios of the two tripeptides, Fmoc-FFC and Fmoc-FFK, and of the aromatic dipeptide Fmoc-FF. The examined ratios for mixed hydrogels were 1/1, 1/5, 1/10, and 1/20 *w/w*. Stock solutions of each peptide were prepared in DMSO (100 mg·mL<sup>-1</sup>), then mixed, vortexed, and subsequently rehydrated with PNA solutions previously quantified *via* UV-Vis spectroscopy as described above and dissolved in doubly distilled water, filtered with 22 µm filter diameter. During the rehydration step, the mixtures were additionally stirred for ~3 seconds to promote the homogeneity of the samples. The formation of hydrogels was macroscopically assessed *via* inverted test tube. Furthermore, 150 µL of all samples were analyzed as a function of time during the opaque-limpid transition phase using multiwell 96 plates in the long range (600 nm) to determine the gelation times of the hydrogels following the addition of PNA molecules. The instrument employed was a Victor Nivo PerkinElmer plate reader.

#### 4.4. Rheology

Rheological measurements of freshly preformed PNA-loaded hydrogels (500 µL) at 1.0 wt% were performed with a rotational controlled-stress rheometer (Malvern Kinexus, UK) equipped with a 1.5 cm diameter flat-plate geometry (PU20-PL61). Each analysis was carried out in accordance with the previously mentioned setup. [44] The rheological profiles, reported in Pascal (Pa), were plotted as storage or elastic modulus ( $G'$ ) and shear loss or viscous modulus ( $G''$ ).

#### 4.5. Hydrogel Stability Studies

The determination of hydrogel degradation profile with or without the presence of PNAs was performed by an *in vitro* stability assay, used for evaluating the percentage weight loss of the matrices. Freshly formed 1.0 wt % hydrogels (300 µL) were weighted ( $W_0$ ) and then incubated at 40 °C with 900 µL of Ringer's solution (8.6 mg of NaCl, 0.30 mg of KCl, and 0.33 mg of CaCl<sub>2</sub>). [45] The Ringer's solution was taken out after seven days, and the hydrogels were once more weighed ( $W_t$ ). The following formula was used to represent the degree of degradation as a percentage ratio ( $\Delta W$ ) between the hydrogel weight before ( $W_0$ ) and after ( $W_t$ ) the treatment

$$\Delta W = \left(1 - \frac{W_t}{W_0}\right) \times 100 \quad (1)$$

#### 4.6. Swelling Kinetics

The swelling kinetics of the matrix were evaluated over 24 hours at 25°C. Swelling ratios ( $q$ ), expressed as a percentage, were evaluated by adding 600 µL of double-distilled water to 300 µL of

freshly prepared hydrogel (1.0 % wt). After removing excess water, for each time point,  $q$  was estimated using equation (2).  $W_s$  and  $W_d$  indicate the weight of the fully swollen hydrogel obtained after removal of excess water and lyophilized samples, respectively.

$$q = \left( \frac{W_s}{W_d} - 1 \right) \times 100 \quad (2)$$

#### 4.7. Circular Dichroism (CD) Spectroscopy

CD spectra of all the peptide-based multicomponent materials in combination with PNA solutions 50  $\mu$ M were recorded in the 320–190 nm spectral region. Each sample was allocated in a 0.2 mm quartz cell equilibrated at 25 °C. Measurements were performed on a Jasco J-1500-150 spectropolarimeter equipped with a Jasco MCB-100 Mini Water Circulation Bath thermal controller unit (Peltier device), as previously described. [44] All the HGs were investigated in combination with PNA solutions.

#### 4.8. Fourier Transform Infrared Spectroscopy (FT-IR)

FT-IR spectra of all the 1.0 wt% peptide-based hydrogels in combination with 50  $\mu$ M PNA solutions were performed on a Jasco FT/IR 4100 spectrometer (Easton, MD, USA) as previously described. [46] After collection in transmission mode, amide I absorbance profiles (in the 1700–1600  $\text{cm}^{-1}$  region) were automatically returned as emissions by the instrument's integrated software, namely secondary structure analysis (SSE) software for Infrared Interpretation and modeling of proteins, version 2.15B.

#### 4.9. Peptides and PNAs $^1\text{H}$ -NMR Spectroscopy

NMR experiments were recorded on an Avance Neo (600 MHz) spectrometer equipped with an HCN triple resonance CryoProbe (Bruker-Biospin, Billerica, MA, USA) at 298 K. Chemical shifts ( $\delta$ ) are reported in ppm downfield from the residual solvent peak, whereas coupling constants ( $J$ ) are stated in Hz. NMR data processing was performed with MestReNova 14.2.0 software (Mestrelab Research, Santiago de Compostela, Spain). NMR samples of pure Fmoc-FFK (3 mg), Fmoc-FFC (3 mg), PNA-E (1.5 mg), and PNA-C (1.5 mg) were obtained by dissolving the samples in 500  $\mu$ L DMSO- $d_6$ . NMR samples of Fmoc-FFK/Fmoc-FF+PNA-E and Fmoc-FFC/Fmoc-FF+PNA-C hydrogels were prepared directly in NMR tubes using D<sub>2</sub>O/DMSO- $d_6$  (2:1 v/v) and analyzed after gelation. All spectra in aqueous buffers were referenced to the residual H<sub>2</sub>O signal (4.78 ppm at 298 K).

$^1\text{H}$ -NMR of Fmoc-FFK (600 MHz, DMSO, Figure S11) ( $\delta$  8.13 (dd,  $J$  = 15.6, 6.9 Hz, 1H), 8.05 (d,  $J$  = 8.1 Hz, 1H), 7.86 (dd,  $J$  = 21.6, 7.2 Hz, 2H), 7.65–7.55 (m, 2H), 7.41 (q,  $J$  = 7.1 Hz, 2H), 7.24 (dd,  $J$  = 13.6, 6.2 Hz, 6H), 7.08 (s, 1H), 6.28 (s, 0H), 4.59–4.49 (m, 1H), 4.25–4.15 (m, 2H), 4.14–4.06 (m, 1H), 3.04 (ddd,  $J$  = 33.0, 13.9, 4.6 Hz, 1H), 2.91 (dd,  $J$  = 14.0, 3.7 Hz, 1H), 2.78–2.65 (m, 3H), 1.68 (h,  $J$  = 6.3 Hz, 1H), 1.51 (dq,  $J$  = 15.7, 7.0 Hz, 3H), 1.28 (tt,  $J$  = 24.6, 12.2 Hz, 2H).

$^1\text{H}$ -NMR of Fmoc-FFC (600 MHz, DMSO, Figure S12) ( $\delta$  8.33–8.28 (m, 1H), 8.24 (dd,  $J$  = 23.4, 7.7 Hz, 2H), 8.11 (d,  $J$  = 8.1 Hz, 2H), 7.87 (dt,  $J$  = 9.9, 4.9 Hz, 8H), 7.60 (ddt,  $J$  = 20.8, 14.9, 7.4 Hz, 12H), 7.40 (p,  $J$  = 7.7 Hz, 9H), 7.30 (dt,  $J$  = 20.3, 7.7 Hz, 6H), 7.24–7.18 (m, 38H), 7.16–7.12 (m, 2H), 4.59–4.55 (m, 3H), 4.33 (q,  $J$  = 7.0 Hz, 3H), 4.22 (td,  $J$  = 9.6, 4.2 Hz, 4H), 4.18–4.03 (m, 11H), 3.94 (d,  $J$  = 17.8 Hz, 1H), 3.18–3.10 (m, 1H), 3.08–3.01 (m, 2H), 2.96–2.77 (m, 11H), 2.72 (ddd,  $J$  = 13.7, 10.6, 7.0 Hz, 6H), 2.26 (dt,  $J$  = 33.1, 8.0 Hz, 2H), 2.07 (s, 16H), 1.29–1.22 (m, 12H), 1.05 (t,  $J$  = 7.0 Hz, 1H), 0.86 (dt,  $J$  = 13.9, 7.3 Hz, 3H).

$^1\text{H}$ -NMR of PNA-E (600 MHz, DMSO, Figure S13) ( $\delta$  12.68 (s, 1H), 11.36–11.19 (m, 5H), 8.15 (d,  $J$  = 10.5 Hz, 1H), 7.85 (s, 1H), 7.63–7.60 (m, 2H), 7.45–7.40 (m, 1H), 7.28 (d,  $J$  = 6.2 Hz, 3H), 6.81 (s, 1H), 4.67 (dd,  $J$  = 16.8, 5.8 Hz, 3H), 4.53–4.45 (m, 1H), 4.40 (d,  $J$  = 14.0 Hz, 2H), 4.23–4.13 (m, 2H), 4.05–3.98 (m, 6H), 3.90–3.86 (m, 2H), 3.62 (s, 2H), 3.51 (d,  $J$  = 4.7 Hz, 2H), 3.08 (s, 2H), 2.93 (dd,  $J$  = 12.9, 6.5 Hz, 2H), 2.14 (dt,  $J$  = 22.9, 8.1 Hz, 3H), 1.72 (dd,  $J$  = 18.4, 8.5 Hz, 8H), 1.52 (s, 1H), 1.46 (d,  $J$  = 3.9 Hz, 1H), 1.23 (s, 1H).

$^1\text{H}$ -NMR of PNA-C (600 MHz, DMSO, Figure S13)  $\delta$  11.35 – 11.17 (m, 1H), 7.50 – 7.16 (m, 1H), 4.67 (d,  $J$  = 26.9 Hz, 1H), 4.61 – 4.35 (m, 1H), 4.02 (d,  $J$  = 23.0 Hz, 1H), 3.40 – 3.35 (m, 191H), 1.76 – 1.67 (m, 2H), 1.62 (td,  $J$  = 21.0, 7.3 Hz, 1H).

#### 4.10. Fluorescence Spectroscopic Assay

The aggregation behavior of mixed hydrogels in combination with PNA-FITC solutions was assessed using a spectroscopic assay. Hydrogels (200  $\mu\text{L}$ ) were prepared according to the solvent-switch method, as reported above, by using PNA solutions [25  $\mu\text{M}$ ]. After gel formation,  $\sim 150$   $\mu\text{L}$  of the samples were deposited on a clean coverslip glass and let to dry overnight. The dried stained films, or xerogels, were observed under bright-field illumination and in the spectral region of the FITC fluorophore ( $\lambda_{\text{exc}}$  = 488 nm,  $\lambda_{\text{em}}$  = 520 nm). [47] Scale bars were acquired with a magnification of 100  $\mu\text{m}$  for all the pictures. Fluorescence images were taken with a Leica MICA micro-hub fluorescence microscope equipped with a 10X objective.

#### 4.11. Scanning Electron Microscopy (SEM)

Morphological analysis of xerogels was carried out by field-emission SEM on a Phenom ProX instrument (Alfatest, Milan, Italy) as previously described. [10,11] The analyses were carried out on samples previously prepared by drop-casting 40  $\mu\text{L}$  of each multicomponent peptide hydrogel combined with PNAs [50  $\mu\text{M}$ ] on an aluminum pin stub, whereas 20  $\mu\text{L}$  were used for PNAs solutions [50  $\mu\text{M}$ ].

#### 4.12. Release and Permeation Studies of PNAs

Using the previously described method, conical tubes containing PNA-FITC encapsulating HGs (400  $\mu\text{L}$ ) were prepared. Each peptide's DMSO solution was rehydrated using a PNA-FITC water solution at a concentration of 0.00015 mol  $\text{L}^{-1}$ . Using UV-Vis spectroscopy, the concentration of PNA solutions ( $\epsilon_{490}$  = 48900  $\text{L}\cdot\text{cm}^{-1}$ ) was quantitatively measured. Each hydrogel with PNA-K was covered with a total of 800  $\mu\text{L}$  of water, while the hydrogel with PNA-C was covered with 800  $\mu\text{L}$  of a 20 mM DTT water solution [15]. At predefined intervals, 400  $\mu\text{L}$  of this solution was withdrawn and replaced with 400  $\mu\text{L}$  of fresh water. The amount of PNAs in each fraction was followed over 10 days and estimated *via* UV-vis spectroscopy using a NanoPhotometer® NP80 Nanodrop (Implen, Munich, Germany). The results were then expressed as a percentage of the ratio between the initial amount that was encapsulated and the released PNAs. Permeation assays were performed by incubating 400  $\mu\text{L}$  of preformed hydrogels in conical tubes 1.5 mL with 800  $\mu\text{L}$  of PNA-FITC solution 0.00015 mol  $\text{L}^{-1}$ . Hydrogels' permeation was followed over 72 h.

**Supplementary Materials:** “The following supporting information can be downloaded at the website of this paper posted on Preprints.org, Figure S1: Physicochemical characterization of PNA-E; Figure S2: Physicochemical characterization of PNA-E\*; Figure S3: Physicochemical characterization of PNA-C; Figure S4: Physicochemical characterization of PNA-C\*; Figure S5: UV-Vis profiles of PNA-functionalized Fmoc-FFX/Fmoc-FF mixed hydrogels; Figure S6: Rheological analysis of PNA-functionalized Fmoc-FFX/Fmoc-FF mixed hydrogels; Figure S7: Swelling kinetics for Fmoc-FFK/Fmoc-FF and Fmoc-FFC/Fmoc-FF matrices; Figure S8: Swelling kinetics for Fmoc-FFK/Fmoc-FF and Fmoc-FFC/Fmoc-FF matrices containing PNA-C and PNA-E; Figure S9: CD spectra of PNA-E and PNA-C; Figure S10: FT-IR absorbance spectra in the Amide I region of PNA-E and PNA-C; Figure S11:  $^1\text{H}$ -NMR spectrum of Fmoc-FFK; Figure S12:  $^1\text{H}$ -NMR spectrum of Fmoc-FFC; Figure S13:  $^1\text{H}$ -NMR spectrum of PNA-C and PNA-E; Figure S14: Physicochemical characterization of Fmoc-FFC-S-S-cys-PNA (1.0 EQ) via ESI mass spectrometry (Enhanced Resolution).

**Author Contributions:** Conceptualization, G.P., N.B., and G.O.; methodology, S.G., M.T., E.G., C.D., and A.P.F.; formal analysis, S.G., M.F., M.S., and N.B.; investigation, S.G., M.T., N.B., and G.O.; resources, G.P., M.S., and G.O.; data curation, S.G., A.A., and G.O.; writing—original draft preparation, S.G., M.T., A.P.F., and G.O.;



writing—review and editing, N.B., A.A., and G.O.; supervision, G.O.; funding acquisition, N.B., G.P., and G.O. All authors have read and agreed to the published version of the manuscript.

**Funding:** This research was funded by the European Union NextGenerationEU, IR0000010 “ELIXIRxNextGenIT”, National Recovery and Resilience Plan (NRRP), Mission 4 Component 2 Investment 3.1, CUP UNINA: B53C22001800006, and CN00000041 “National Center for Gene Therapy and Drugs based on RNA Technology”, National Recovery and Resilience Plan (NRRP), Mission 4 Component 2 Investment 1.4, CUP UNINA: E63C22000940007.

**Data Availability Statement:** Data is contained within the article and supplementary material.

**Acknowledgments:** The authors are grateful to Dr Maria Marzano for technical assistance.

**Conflicts of Interest:** The authors declare no conflicts of interest.

## References

1. Zhang, C.; Yan, L.; Wang, X.; Zhu, S.; Chen, C.; Gu, Z.; Zhao, Y. Progress, Challenges, and Future of Nanomedicine. *Nano Today* 2020, 35, 101008, doi:10.1016/j.nantod.2020.101008.
2. Mondal, S.; Das, S.; Nandi, A.K. A Review on Recent Advances in Polymer and Peptide Hydrogels. *Soft Matter* 2020, 16, 1404–1454, doi:10.1039/C9SM02127B.
3. Karchoubi, F.; Afshar Ghotli, R.; Pahlevani, H.; Baghban Salehi, M. New Insights into Nanocomposite Hydrogels; a Review on Recent Advances in Characteristics and Applications. *Advanced Industrial and Engineering Polymer Research* 2024, 7, 54–78, doi:10.1016/j.aiepr.2023.06.002.
4. Binaymotlagh, R.; Chronopoulou, L.; Haghighi, F.H.; Fratoddi, I.; Palocci, C. Peptide-Based Hydrogels: New Materials for Biosensing and Biomedical Applications. *Materials* 2022, 15, 5871, doi:10.3390/ma15175871.
5. Das, S.; Das, D. Rational Design of Peptide-Based Smart Hydrogels for Therapeutic Applications. *Front Chem* 2021, 9, doi:10.3389/fchem.2021.770102.
6. Park, S.; Kim, S.H.; Dezhbord, M.; Lee, E.-H.; Jeon, Y.; Jung, D.; Gu, S.H.; Yu, C.; Lee, S.H.; Kim, S.C.; et al. Cell-Permeable Peptide Nucleic Acid Antisense Oligonucleotide Platform Targeting Human Betacoronaviruses. *Front Microbiol* 2023, 14, doi:10.3389/fmicb.2023.1258091.
7. Diaferia, C.; Rosa, E.; Gallo, E.; Morelli, G.; Accardo, A. Differently N-Capped Analogues of Fmoc-FF. *Chemistry – A European Journal* 2023, 29, doi:10.1002/chem.202300661.
8. Wang, Y.; Geng, Q.; Zhang, Y.; Adler-Abramovich, L.; Fan, X.; Mei, D.; Gazit, E.; Tao, K. Fmoc-Diphenylalanine Gelating Nanoarchitectonics: A Simplistic Peptide Self-Assembly to Meet Complex Applications. *J Colloid Interface Sci* 2023, 636, 113–133, doi:10.1016/j.jcis.2022.12.166.
9. Choe, R.; Il Yun, S. Fmoc-Diphenylalanine-Based Hydrogels as a Potential Carrier for Drug Delivery. *e-Polymers* 2020, 20, 458–468, doi:10.1515/epoly-2020-0050.
10. Giordano, S.; Gallo, E.; Diaferia, C.; Rosa, E.; Carrese, B.; Borbone, N.; Scognamiglio, P.L.; Franzese, M.; Oliviero, G.; Accardo, A. Multicomponent Peptide-Based Hydrogels Containing Chemical Functional Groups as Innovative Platforms for Biotechnological Applications. *Gels* 2023, 9, 903, doi:10.3390/gels9110903.
11. Gallo, E.; Diaferia, C.; Giordano, S.; Rosa, E.; Carrese, B.; Piccialli, G.; Borbone, N.; Morelli, G.; Oliviero, G.; Accardo, A. Ultrashort Cationic Peptide Fmoc-FFK as Hydrogel Building Block for Potential Biomedical Applications. *Gels* 2023, 10, 12, doi:10.3390/gels10010012.
12. Uhlmann, E.; Peyman, A.; Breipohl, G.; Will, D.W. PNA: Synthetic Polyamide Nucleic Acids with Unusual Binding Properties. *Angewandte Chemie International Edition* 1998, 37, 2796–2823, doi:10.1002/(SICI)1521-3773(19981102)37:20<2796::AID-ANIE2796>3.0.CO;2-K.
13. Falanga, A.P.; Cerullo, V.; Marzano, M.; Feola, S.; Oliviero, G.; Piccialli, G.; Borbone, N. Peptide Nucleic Acid-Functionalized Adenoviral Vectors Targeting G-Quadruplexes in the P1 Promoter of Bcl-2 Proto-Oncogene: A New Tool for Gene Modulation in Anticancer Therapy. *Bioconj Chem* 2019, 30, 572–582, doi:10.1021/acs.bioconjchem.8b00674.
14. Hanvey, J.C.; Peffer, N.J.; Bisi, J.E.; Thomson, S.A.; Cadilla, R.; Josey, J.A.; Ricca, D.J.; Hassman, C.F.; Bonham, M.A.; Au, K.G.; et al. Antisense and Antigene Properties of Peptide Nucleic Acids. *Science* (1979) 1992, 258, 1481–1485, doi:10.1126/science.1279811.

15. Terracciano, M.; Fontana, F.; Falanga, A.P.; D'Errico, S.; Torrieri, G.; Greco, F.; Tramontano, C.; Rea, I.; Piccialli, G.; De Stefano, L.; et al. Development of Surface Chemical Strategies for Synthesizing Redox-Responsive Diatomite Nanoparticles as a Green Platform for On-Demand Intracellular Release of an Antisense Peptide Nucleic Acid Anticancer Agent. *Small* 2022, 18, doi:10.1002/sml.202204732.
16. MacLelland, V.; Kravitz, M.; Gupta, A. Therapeutic and Diagnostic Applications of Antisense Peptide Nucleic Acids. *Mol Ther Nucleic Acids* 2024, 35, 102086, doi:10.1016/j.omtn.2023.102086.
17. Falanga, A.P.; Greco, F.; Terracciano, M.; D'Errico, S.; Marzano, M.; Feola, S.; Sepe, V.; Fontana, F.; Piccialli, I.; Cerullo, V.; et al. Engineering an Oncolytic Adenoviral Platform for Precise Delivery of Antisense Peptide Nucleic Acid to Modulate PD-L1 Overexpression in Cancer Cells. *Int J Pharm* 2025, 668, 124941, doi:10.1016/j.ijpharm.2024.124941.
18. Zarrilli, F.; Amato, F.; Morgillo, C.M.; Pinto, B.; Santaripa, G.; Borbone, N.; D'Errico, S.; Catalanotti, B.; Piccialli, G.; Castaldo, G.; et al. Peptide Nucleic Acids as MiRNA Target Protectors for the Treatment of Cystic Fibrosis. *Molecules* 2017, 22, 1144, doi:10.3390/molecules22071144.
19. Gaglione, M.; Milano, G.; Chambery, A.; Moggio, L.; Romanelli, A.; Messere, A. PNA-Based Artificial Nucleases as Antisense and Anti-MiRNA Oligonucleotide Agents. *Mol Biosyst* 2011, 7, 2490, doi:10.1039/c1mb05131h.
20. Moretta, R.; Terracciano, M.; Borbone, N.; Oliviero, G.; Schiattarella, C.; Piccialli, G.; Falanga, A.P.; Marzano, M.; Dardano, P.; De Stefano, L.; et al. PNA-Based Graphene Oxide/Porous Silicon Hybrid Biosensor: Towards a Label-Free Optical Assay for Brugada Syndrome. *Nanomaterials* 2020, 10, 2233, doi:10.3390/nano10112233.
21. Crisci, T.; Falanga, A.P.; Casalino, M.; Borbone, N.; Terracciano, M.; Chianese, G.; Giofrè, M.; D'Errico, S.; Marzano, M.; Rea, I.; et al. Bioconjugation of a PNA Probe to Zinc Oxide Nanowires for Label-Free Sensing. *Nanomaterials* 2021, 11, 523, doi:10.3390/nano11020523.
22. Pooga, M.; Land, T.; Bartfai, T.; Langel, Ü. PNA Oligomers as Tools for Specific Modulation of Gene Expression. *Biomol Eng* 2001, 17, 183–192, doi:10.1016/S1389-0344(01)00075-2.
23. Berger, S.; Lächelt, U.; Wagner, E. Dynamic Carriers for Therapeutic RNA Delivery. *Proceedings of the National Academy of Sciences* 2024, 121, doi:10.1073/pnas.2307799120.
24. Gupta, A.; Bahal, R.; Gupta, M.; Glazer, P.M.; Saltzman, W.M. Nanotechnology for Delivery of Peptide Nucleic Acids (PNAs). *Journal of Controlled Release* 2016, 240, 302–311, doi:10.1016/j.jconrel.2016.01.005.
25. Ambasht, P.K. Use of Group-Specific Reagents in Active Site Functional Group Elucidation I: Cys, Ser, Tyr, and Trp Residues. In *Frontiers in Protein Structure, Function, and Dynamics*; Springer Singapore: Singapore, 2020; pp. 71–94.
26. Choi, H.; Go, M.; Cha, Y.; Choi, Y.; Kwon, K.-Y.; Jung, J.H. A Facile Method to Fabricate Hydrogels from DMSO Polymer Gels via Solvent Exchange. *New Journal of Chemistry* 2017, 41, 4793–4796, doi:10.1039/C7NJ00152E.
27. Tang, C.; Smith, A.M.; Collins, R.F.; Ulijn, R. V.; Saiani, A. Fmoc-Diphenylalanine Self-Assembly Mechanism Induces Apparent p K a Shifts. *Langmuir* 2009, 25, 9447–9453, doi:10.1021/la900653q.
28. Katouezadeh, E.; Rasouli, M.; Zebarjad, S.M. The Rheological Behavior of the Non-Newtonian Thixotropic Colloidal Silica Gels from Sodium Silicate. *Mater Chem Phys* 2021, 272, 124994, doi:10.1016/j.matchemphys.2021.124994.
29. Stojkov, G.; Niyazov, Z.; Picchioni, F.; Bose, R.K. Relationship between Structure and Rheology of Hydrogels for Various Applications. *Gels* 2021, 7, 255, doi:10.3390/gels7040255.
30. Adams, D.J.; Mullen, L.M.; Berta, M.; Chen, L.; Frith, W.J. Relationship between Molecular Structure, Gelation Behaviour and Gel Properties of Fmoc-Dipeptides. *Soft Matter* 2010, 6, 1971, doi:10.1039/b921863g.
31. Orbach, R.; Mironi-Harpaz, I.; Adler-Abramovich, L.; Mossou, E.; Mitchell, E.P.; Forsyth, V.T.; Gazit, E.; Seliktar, D. The Rheological and Structural Properties of Fmoc-Peptide-Based Hydrogels: The Effect of Aromatic Molecular Architecture on Self-Assembly and Physical Characteristics. *Langmuir* 2012, 28, 2015–2022, doi:10.1021/la204426q.
32. Chronopoulou, L.; Margheritelli, S.; Toumia, Y.; Paradossi, G.; Bordini, F.; Sennato, S.; Palocci, C. Biosynthesis and Characterization of Cross-Linked Fmoc Peptide-Based Hydrogels for Drug Delivery Applications. *Gels* 2015, 1, 179–193, doi:10.3390/gels1020179.

33. Chin, D.-H.; Woody, R.W.; Rohl, C.A.; Baldwin, R.L. Circular Dichroism Spectra of Short, Fixed-Nucleus Alanine Helices. *Proceedings of the National Academy of Sciences* 2002, *99*, 15416–15421, doi:10.1073/pnas.232591399.
34. Sahoo, J.K.; Roy, S.; Javid, N.; Duncan, K.; Aitken, L.; Ulijn, R. V. Pathway-Dependent Gold Nanoparticle Formation by Biocatalytic Self-Assembly. *Nanoscale* 2017, *9*, 12330–12334, doi:10.1039/C7NR04624C.
35. Wang, Y.; Geng, Q.; Zhang, Y.; Adler-Abramovich, L.; Fan, X.; Mei, D.; Gazit, E.; Tao, K. Fmoc-Diphenylalanine Gelating Nanoarchitectonics: A Simplistic Peptide Self-Assembly to Meet Complex Applications. *J Colloid Interface Sci* 2023, *636*, 113–133, doi:10.1016/j.jcis.2022.12.166.
36. Ryan, K.; Beirne, J.; Redmond, G.; Kilpatrick, J.I.; Guyonnet, J.; Buchete, N.-V.; Kholkin, A.L.; Rodriguez, B.J. Nanoscale Piezoelectric Properties of Self-Assembled Fmoc-FF Peptide Fibrous Networks. *ACS Appl Mater Interfaces* 2015, *7*, 12702–12707, doi:10.1021/acsami.5b01251.
37. Goormaghtigh, E.; Ruysschaert, J.-M.; Raussens, V. Evaluation of the Information Content in Infrared Spectra for Protein Secondary Structure Determination. *Biophys J* 2006, *90*, 2946–2957, doi:10.1529/biophysj.105.072017.
38. Zandomenighi, G.; Krebs, M.R.H.; McCammon, M.G.; Fändrich, M. FTIR Reveals Structural Differences between Native B-sheet Proteins and Amyloid Fibrils. *Protein Science* 2004, *13*, 3314–3321, doi:10.1110/ps.041024904.
39. Arrondo, J.L.R.; Goñi, F.M. Structure and Dynamics of Membrane Proteins as Studied by Infrared Spectroscopy. *Prog Biophys Mol Biol* 1999, *72*, 367–405, doi:10.1016/S0079-6107(99)00007-3.
40. Sardaru, M.-C.; Marangoci, N.-L.; Palumbo, R.; Roviello, G.N.; Rotaru, A. Nucleic Acid Probes in Bio-Imaging and Diagnostics: Recent Advances in ODN-Based Fluorescent and Surface-Enhanced Raman Scattering Nanoparticle and Nanostructured Systems. *Molecules* 2023, *28*, 3561, doi:10.3390/molecules28083561.
41. Lakshmanan, A.; Cheong, D.W.; Accardo, A.; Di Fabrizio, E.; Riekel, C.; Hauser, C.A.E. Aliphatic Peptides Show Similar Self-Assembly to Amyloid Core Sequences, Challenging the Importance of Aromatic Interactions in Amyloidosis. *Proceedings of the National Academy of Sciences* 2013, *110*, 519–524, doi:10.1073/pnas.1217742110.
42. McFetridge, M.L.; Kulkarni, K.; Hilsenstein, V.; Del Borgo, M.P.; Aguilar, M.-I.; Ricardo, S.D. A Comparison of Fixation Methods for SEM Analysis of Self-Assembling Peptide Hydrogel Nanoarchitecture. *Nanoscale* 2023, *15*, 1431–1440, doi:10.1039/D2NR04598B.
43. Coin, I.; Beyermann, M.; Bienert, M. Solid-Phase Peptide Synthesis: From Standard Procedures to the Synthesis of Difficult Sequences. *Nat Protoc* 2007, *2*, 3247–3256, doi:10.1038/nprot.2007.454.
44. Rosa, E.; Gallo, E.; Sibillano, T.; Giannini, C.; Rizzuti, S.; Gianolio, E.; Scognamiglio, P.L.; Morelli, G.; Accardo, A.; Diaferia, C. Incorporation of PEG Diacrylates (PEGDA) Generates Hybrid Fmoc-FF Hydrogel Matrices. *Gels* 2022, *8*, 831, doi:10.3390/gels8120831.
45. Sunde, M.; Serpell, L.C.; Bartlam, M.; Fraser, P.E.; Pepys, M.B.; Blake, C.C.F. Common Core Structure of Amyloid Fibrils by Synchrotron X-Ray Diffraction 1 Edited by F. E. Cohen. *J Mol Biol* 1997, *273*, 729–739, doi:10.1006/jmbi.1997.1348.
46. Diaferia, C.; Rosa, E.; Gallo, E.; Smaldone, G.; Stornaiuolo, M.; Morelli, G.; Accardo, A. Self-Supporting Hydrogels Based on Fmoc-Derivatized Cationic Hexapeptides for Potential Biomedical Applications. *Biomedicines* 2021, *9*, 678, doi:10.3390/biomedicines9060678.
47. Jorbágy, A.; Király, K. Chemical Characterization of Fluorescein Isothiocyanate-Protein Conjugates. *Biochimica et Biophysica Acta (BBA) - General Subjects* 1966, *124*, 166–175, doi:10.1016/0304-4165(66)90325-4.

**Disclaimer/Publisher's Note:** The statements, opinions and data contained in all publications are solely those of the individual author(s) and contributor(s) and not of MDPI and/or the editor(s). MDPI and/or the editor(s) disclaim responsibility for any injury to people or property resulting from any ideas, methods, instructions or products referred to in the content.